Computational Chemistry Considerations in Catalysis: Regioselectivity and Metal-Ligand Dissociation

Prajay Patel, Angela K. Wilson*

Department of Chemistry, Michigan State University, East Lansing, Michigan 48824, U.S.A.

Key words: computational chemistry, DFT, catalysis, CCSD(T), hydroformylation

ABSTRACT

The utility of a range of computational chemistry approaches for the prediction of the regioselectivity for hydroformylation processes and metal-ligand dissociation in a model organometallic system is considered to provide insight about computational strategies for use in catalysis. The hydroformylation reactions investigated are the Rh-catalyzed hydroformylation of terminal alkenes with triarylphosphine and chelating diphosphine ligands. As well, the dissociation of water from a Pt complex is considered to probe method effects on metal-ligand bonding. Several density functional theory (DFT) approaches and *ab initio* methods are considered. We demonstrate that the quality of the basis set selected for the calculations can play a vital role in the prediction of even the product distribution, and that correcting for basis set superposition error (BSSE) can be very important. As well, the study demonstrates a broad range of predictions achievable using a variety of DFT approaches, which is, as discussed, a manifestation of the challenges that are encountered for calculations involving transition metal molecular species, illustrating the critical need to gauge computational chemistry methods.

1. Introduction

Computational chemistry can provide a useful partner to experiment in the discovery, development, and characterization of new possible catalysts and catalytic processes, and the refinement of existing catalysts and catalytic processes. Key to the utility, however, are a number of factors including reliability, reproducibility, and transferability. Gauging computational methods is just as important as it is to calibrate instrumentation used in experiments, or insuring yield from a synthetic process, yet, an unfortunate practice is to simply utilize the most popular computational method. Computational methods can vary widely in their utility and their computational cost (amount of computer time, memory, and disk space required in a calculation), particularly in the realm of transition metals or heavy elements, and as the bulkiness of the catalyst of interest is increased.

For the prediction of thermodynamic information (i.e., enthalpies, free energies), reaction barriers, HOMO-LUMO gaps, and other fundamental properties, density functional theory (DFT) approaches are very commonly used for catalysis. For early main group chemistry (i.e., hydrocarbons), there are many different forms of DFT – called density functionals – that can be used quite easily, with very little difference in predicted property arising from the choice of functional to describe energetics, and with limited exceptions, as demonstrated by Karton et al. [1] However, for transition metal species, the utility of each functional can vary widely based upon choice of metal, choice of ligand, and property of interest. [2–8] To

* *E-mail address:* akwilson@msu.edu (A.K. Wilson)

illustrate, for a set of ~20 3*d* transition metal species, B3LYP/CEP-31G(d) resulted in errors from experiment from the predicted enthalpies of formation by ~100 kcal mol^{-1}. [2]

However, when the same functional is applied to a different set of the transition metal species – a set that has the smallest reported experimental uncertainties in the enthalpy of formation – the error is ~6-7 kcal mol^{-1}. [4,5] So, indeed, extraordinarily large variances can occur depending upon metal and ligand. However, for catalysis, where there may be interest in understanding the thermochemistry with much smaller errors in energy, this magnitude of error may be of limited utility. Computational approaches have been designed to improve upon the predictions possible by DFT for these benchmark thermochemical data for transition metal species. With *ab initio* composite approaches like the correlation consistent Composite Approach, ccCA, designed in our group, [9–13] differences of ~2-3 kcal mol^{-1}, on average, can be achieved in the prediction of enthalpies of formation for 3*d* transition metal species. [12,13] As well, ccCA targeted 4*d* transition metal chemistry by utilizing relativistic pseudopotentials, denoted as rp-ccCA, to model relativistic contributions from core electrons and yielded differences of ~3 kcal mol^{-1} from experimental enthalpies of formation. [10,13] This is useful, but more costly than DFT approaches. Strategies have evolved that help to reduce the bottleneck in these calculations (e.g., DLPNO-ccCA) - computational cost - while preserving the accuracy in the energetic predictions. And, thus, this approach can be quite useful as a route to either gauge DFT approaches in the absence of experiment, or, as a means to provide quantitative energy predictions for studies of homogeneous processes (or for problems that can be well-representative by a homogeneous process).

So far, these comments have focused upon general trends in the prediction of thermodynamic properties of molecular systems. However, a question is, what is the utility of computational approaches for an important industrial process like hydroformylation? More specifically, how useful are computational approaches, particularly new approaches like DLPNO-ccCA, a form of ccCA, for important properties like regioselectivity and metal-ligand binding? And, is the qualitative or quantitative picture impacted by computational method choice?

The mechanism for Rh-based hydroformylation was well-established by Wilkinson in the late 1960s to early 1970s. [14] As the largest volume homogeneous chemical reaction conducted in industry for chemical production, the process converts olefins to aldehydes in a syngas mixture. The advantage of Rh-based hydroformylation as opposed to Co-based hydroformylation is the favorable reaction conditions (ambient temperature and pressure). The efficacy of a catalyst designed for hydroformylation is the ratio of the linear aldehyde to the branched aldehyde (Fig. 1), known as the linear-to-branched ratio. In hydroformylation, the formation of the linear aldehyde is favored although there are studies targeting asymmetric hydroformylation, i.e. the production of the branched aldehyde. [15,16] This is measured through the kinetics of the migratory insertion of the olefin to the catalyst.

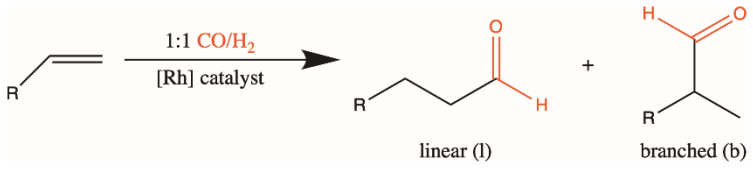

Figure 1. Hydroformylation reaction converting olefins to linear and branched aldehydes via a Rh catalyst.

Numerous computational studies have targeted modeling the regioselectivity of hydroformylation due to its importance in chemical industry. [17–26] To account for the size of the catalysts and the limited computing power at the time, earlier computational studies either substituted PPh_3 ligands with much

smaller PH_3 ligands or utilized multilevel computational chemistry methods, such as ONIOM, [27,28] to model the bond breaking and formation region with DFT while relegating the sterically bulky ligands to a computationally more affordable method, such as molecular mechanics (MM). [17–21] While more recent studies also utilize multilevel approaches for hydroformylation, more rigorous *ab initio* methodologies are used to model bond breaking and forming regions and use DFT to model the steric ligands. [22,23] Other studies have only used DFT to model the olefin insertion step as well as the entire Wilkinson catalytic cycle. [23–25,29,30] These studies provide insight into potential electronic contributions of the sterically bulky ligands as well as the mechanism by identifying the rate-determining step, which can change based on the type of ligand. Machine learning approaches have recently been developed to screen potential ligands based on their regioselectivity and is a rising trend in computational catalysis. [26,31]

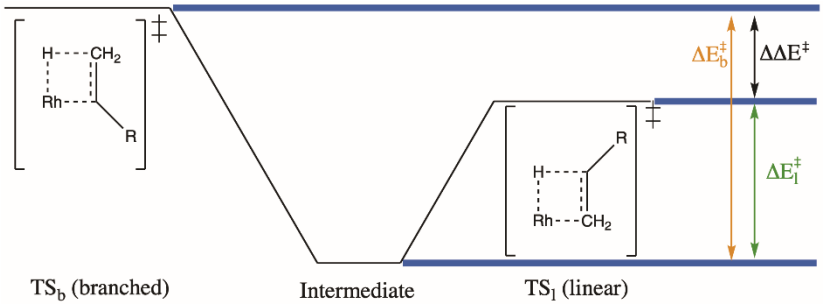

Figure 2. A model of the two reaction pathways for hydroformylation where $\Delta E_l^{\ddagger}$ and $\Delta E_b^{\ddagger}$ are the reaction barrier for forming the linear and branched product, respectively. $\Delta\Delta E^{\ddagger}$ is the difference in energy between the two reaction barriers.

The kinetics of hydroformylation is very sensitive energetically, i.e. the differences in energy between competing pathways ($\Delta\Delta E^{\ddagger}$), illustrated in Fig. 2, can be less than 1 kcal mol^{-1}. [17] With such small differences in energy for the competing pathways, calculating the correct linear-to-branched ratio can be difficult to predict with computational methods. For example, as shown in Table 1, if $\Delta\Delta E^{\ddagger} = 0$ (reaction barriers are equivalent), the l:b ratio is 50:50. However, lowering the barrier for the linear product by 1 kcal mol^{-1} ($\Delta\Delta E^{\ddagger}$ = -1 kcal mol^{-1}) results in a product ratio increase to approximately 84:16 and lowering the barrier for the formation of the linear product by an additional 2 kcal mol^{-1} ($\Delta\Delta E^{\ddagger}$= -3 kcal mol^{-1}) indicates that the reaction highly favors the linear product (100:0 ratio). Therefore, to investigate the regioselectivity of hydroformylation, a [Rh(H)(CO)] backbone was considered with both mono- and bidentate phosphine ligands.

Table 1. Summary of the effect of $\Delta\Delta E^{\ddagger}$ in kcal mol^{-1} on the linear-to-branched ratio (l:b) ratio for hydroformylation.

$\Delta\Delta E^{\ddagger}$ (kcal mol^{-1})	Linear-to-branched ratio (l:b)
0 to -1	50:50 to 84:16
1 to -2	84:16 to 97:3
-2 to -3	97:3 to 100:0

Basically, considering the challenges mentioned earlier about the prediction of thermochemistry properties for transition metal species, achieving the level of accuracy needed to even predict the correct product distributions seems unsurmountable. Cancellation of errors that can occur from comparing energy differences is helpful, though the errors from experiment are not necessarily the same across a reaction pathway, and, thus, gauging method utility for each problem, considering metal, ligand, and property, is essential. Thus, in this study, the impact of method and basis set choice – the route to describe the molecular orbitals – are considered to determine the impact of these choices upon the prediction of linear-to-branched

ligand ratio, as well as the ligand dissociation energy. The hydroformylation reactions investigated are the Rh-catalyzed hydroformylation of terminal alkenes using a [Rh(H)(CO)] backbone with mono- (PPh_3) and bidentate phosphine ligands (TBDCP, DIOP, DIPHOS) as shown in Figures 3 and 4.

Another aspect that is important in catalysis is the description of metal-ligand dissociation, as it is a primary step in all homogeneous catalytic reactions, e.g. product dissociation from Rh-catalyzed hydroformylation and solvent interactions with olefin hydrogenation, as well as gas phase ligand dissociation for organometallic reactions targeting C-H activation. Here, to gain understanding about the utility of the *ab initio* composite strategy, DLPNO-ccCA, a cationic (diimine)(aquo)Pt^{II} complex was examined. This Pt^{II} complex was chosen since Pt^{II} complexes with ligands containing aromatic and aliphatic C-H bonds are involved in the oxidative addition of alkanes and have been a focus in C-H activation studies where the ligand substitution step is rate-determining. [32–35]

2. Computational Methods

2.1 Computational methods for hydroformylation. DFT and *ab initio* calculations were done in this study. Several density functionals were utilized, selecting a number of widely used functionals varying in complexity: B3LYP, [36,37] B3P86, [36,38] BLYP, [37,39] BP86, [38,39] PBE, [40,41] and PBE0. [40–42] (It should be noted that while increased complexity often means better property predictions, this is not necessarily guaranteed.) Grimme's dispersion correction with Becke-Johnson dampening (D3BJ) was included for B3LYP and PBE0 to correct for long-range intramolecular interactions. [43] The Stuttgart/Dresden basis set, and pseudopotential (SDD) was used for all DFT calculations. [44,45] Though it is commonly believed that a triple-ξ quality basis set is sufficient for DFT calculations, earlier work has demonstrated that for the predictions of energetic properties of transition metal species, quadruple-ξ level basis sets can have an impact on the energies, and, thus, this level of basis set was considered.[3,4] As well, this choice of basis set followed earlier work done by Kumar et al. [24], and all structures for the DFT and *ab initio* calculations were based on this prior work. DFT calculations in the present work were done with Gaussian16. [46]

Several *ab initio* correlated methods also were used including domain-based pair natural orbital (DLPNO) methods, [47–52] DLPNO-MP2 and DLPNO-CCSD(T)), the MP2 and CCSD(T) varieties of the DLPNO approach. The DLPNO approach enables computational cost reductions from typical MP2 and CCSD(T) calculations. And, CCSD(T) is of particular interest, as this method is known for its utility in energy predictions when paired with a high-quality (which typically means large) basis set. The DLPNO calculations were done with the ORCA program suite. [53] Calculations were done using Dunning's correlation consistent polarized valence-*n*-ξ ("zeta") basis sets (aug-cc-pV*n*Z, where *n*=D (double), T (triple), Q (quadruple)), and considering augmented (aug-cc-pV*n*Z) and augmented core-valence (aug-cc-pCV*n*Z) forms of the sets. [54,55] For P and Cl, the recommended tight *d* versions of the correlation consistent basis sets, denoted as cc-pV(*n*+*d*)Z, aug-cc-pV(*n*+*d*)Z, and aug-cc-pCV(*n*+*d*)Z were used. [55] The correlation consistent pseudopotentials (cc-pV*n*Z-PP) were used for Rh and Pt atoms. [56,57] The correlation consistent Composite Approach (ccCA) for 4*d* transition metals was also considered, [10] utilizing the DLPNO methods for the composite steps to reduce the computational resources associated with the size of the compound, denoted as DLPNO-rp-ccCA. [58]

To calculate the regioselectivity for hydroformylation, the following equation was used for the linear-to-branched ratio

$$l{:}b = k_l{:}k_b = \exp(-\Delta G_l^{\ddagger}/kT)/\exp((-\Delta G_b^{\ddagger}/kT) = \exp(-\Delta\Delta G^{\ddagger}/kT) \cong \exp(-\Delta\Delta E^{\ddagger}/kT) \quad (1)$$

where $\Delta G^{\ddagger}$ is the free energy barrier, $\Delta\Delta G^{\ddagger}$ is the energy difference between the two reaction pathways, k is the Boltzmann constant, and T is the temperature. This equation assumes the olefin insertion step is irreversible. The Rh-catalyst-olefin complex examined with the DLPNO methods is ee-[Rh(H)(CO)(DIPHOS)(propene)] where the bis-phosphine DIPHOS ligand is in the equatorial-equatorial (ee) coordination mode (shown in Figure 3). The ligands examined with DFT include $(PPh_3)_2$, and more structurally complex bis-phosphine ligands, TBDCP, DIOP, and DIPHOS. All ligands are attached to a [Rh(H)(CO)] backbone as indicated in the Wilkinson catalytic cycle for Rh-based hydroformylation. The ligands are shown in Figure 4. Olefins examined with $(PPh_3)_2$ include pentene, hexene, heptene, octene, decene, dodecene, styrene, and vinyl acetate. Propene is coordinated with all bisphosphine ligands. The ligands are considered in both the equatorial-equatorial (ee) and equatorial-axial (ea) conformations relative to the Rh center. As the experiments were carried out in toluene, the SMD implicit solvent model [59] was used to mimic the long-range solvent effects of toluene on the Rh catalyst.

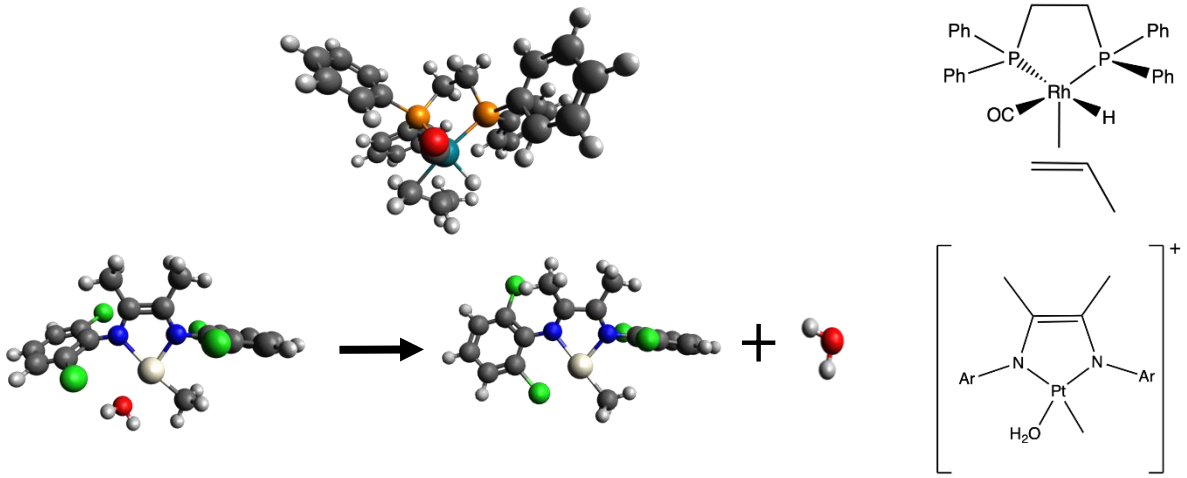

Figure 3. Computationally determined 3D structures (left) and 2D structures (right) of ee-[Rh(H)(CO)(DIPHOS)(propene)] catalyst complex (top) and dissociation reaction of H_2O from the cationic (diimine)(aquo)Pt^{II} complex (bottom). Ph=Phenyl and Ar=2,6-dichlorobenzene. Pt=Silver, N=Blue, O=Red, C=Dark Gray, H=Light Gray, Cl=Green, P=Orange, Rh=Teal.

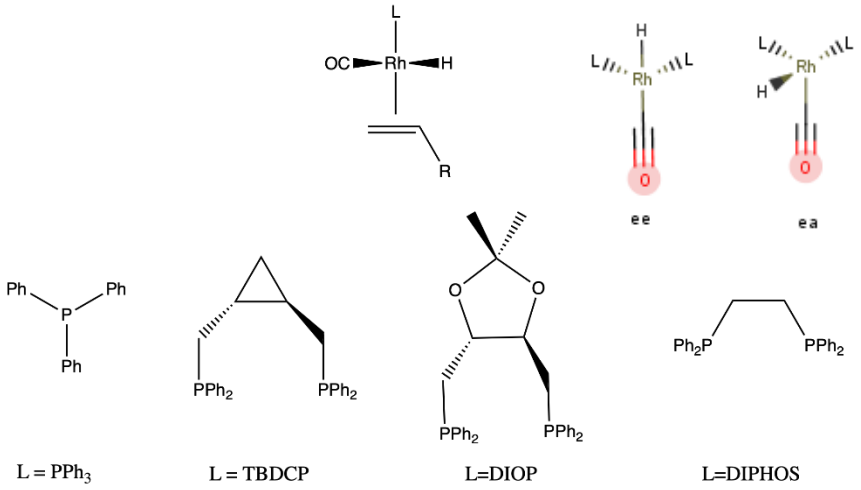

Figure 4. 2D structures of the monodentate and bidentate ligands for hydroformylation as well as the equatorial-equatorial (ee) and equatorial-axial (ea) conformations of the [Rh(H)(CO)] backbone. All ligands are bound to a [Rh(H)(CO)] backbone.

2.2 Computational methods for ligand dissociation. The gas phase ligand dissociation energy was evaluated by the difference between the complex and the respective fragments.

$$\Delta E_{dissoc} = E_{AB} - E_A + E_B \quad (2)$$

where E_{AB} is the electronic energy of the complex, E_A is the electronic energy of fragment A, and E_B is the electronic energy of fragment B. *Ab initio* calculations, in particular, are susceptible to basis set superposition error (BSSE), which can result in overbinding of the ligands, and is applied to all DLPNO calculations for metal-ligand dissociation energy. [60]

To study fundamental organometallic reactions that occur in the gas phase, a cationic (diimine)(aquo)Pt^{II} complex prevalent in C-H activation and oxidative addition of alkanes was chosen (see Fig 3). This molecule was chosen due to computational feasibility based on the molecule size. The calculated zero point energy (ZPE) of the reaction obtained with a frequency calculation at the BP86 level and the PBE0 optimized structures were obtained from Weymuth et al. [61] This choice of functional for frequency calculations was selected since the ZPE of the reaction did not significantly change with respect to functional choice. [61] PBE0 structures were utilized based on their success for heavier elements. A few density functionals, PBE0, B3LYP, and TPSSh [62] utilizing cost-saving techniques, i.e the resolution-of-the-identity or RI approximation, were paired with the augmented correlation consistent basis sets and pseudopotentials of triple- and quadruple-ξ level quality (aug-cc-pV*n*Z, *n*=T, Q), as well as DLPNO-rp-ccCA to determine ligand dissociation energies. All ligand dissociation calculations were done in the ORCA program suite.

3. Results and Discussion

3.1 Regioselectivity in hydroformylation. The DFT l:b ratios for all Rh catalysts are shown in Table 2. The corresponding $\Delta\Delta E^{\ddagger}$s for all DFT results are shown in Table 3. The DLPNO results for hydroformylation are shown in Table 4 for the l:b ratios, including the l:b determined for calculations that have been corrected for BSSE. With DFT, qualitatively correct l:b ratios are obtained for most of the examined catalyst-olefin complexes as shown in Table 2. However, this largely depends on which type of functional is used. For example, using BLYP, BP86, and PBE generally predicted l:b ratios that are in disagreement with experiment for $(PPh_3)_2$ ligands, particularly for hexene, heptene, octene, dodecene, and styrene, which produced l:b ratios of 2:98, 26:74, 11:89, 84:16, and 87:13, respectively, for BLYP, and similar ratios for BP86 and PBE (Table 2). With an increase in complexity in the functionals, i.e. B3LYP, B3P86, and PBE0, l:b ratios of 67:33 47:53 and 76:24 for B3LYP, 71:29, 67:33, 68:32 for B3P86, and 75:25, 73:27, 71:29 for PBE0, were predicted for the conversion of heptane, octene, and dodecane with $(PPh_3)_2$ ligands, respectively. And for ee-[Rh(H)(CO)$(PPh_3)_2$(pentene)], the linear product is predicted. However, the inclusion of Grimme's dispersion correction for B3LYP and PBE0 predicted l:b ratios that predicted the more favorable produce, in agreement with experiment for all examined catalyst-olefin complexes with the exception of ee-[Rh(H)(CO) $(PPh_3)_2$(decene)] (l:b ratios of 0:100 and 3:97 for B3LYP-D3 and PBE0-D3, respectively) and ee-[Rh(H)(CO) (DIPHOS)(propene)] (l:b ratios of 17:83 and 11:89 for B3LYP-D3 and PBE0-D3, respectively). Based on the calculated l:b ratios, predicting regioselectivity with DFT can, but not always, be improved by increasing the complexity of the functional.

Table 2. Comparison of several density functionals to linear-to-branched ratios from experiment for ee-[Rh(H)(CO)(L)(olefin)] complexes

	BLYP	BP86	PBE	B3LYP	B3P86	PBE0	B3LYP-D3	PBE0-D3	Exp [63–70]
L=$(PPh_3)_2$									
Pentene	83:17	81:19	79:21	95:5	95:5	95:5	100:0	99:1	95:5
Hexene	2:98	3:97	6:94	10:90	19:81	23:77	100:0	99:1	92:8
Heptene	26:74	28:72	33:67	67:33	71:29	75:25	100:0	99:1	86:14
Octene	11:89	20:80	31:69	47:53	67:33	73:27	100:0	100:0	81:19
Decene	84:16	93:7	89:11	53:47	69:31	64:36	0:100	3:97	74:26
Dodecene	45:55	33:67	41:59	76:24	68:32	71:29	100:0	99:1	87:12
Styrene	87:13	92:8	79:21	83:17	84:16	90:10	0:100	1:99	11:89
Vinyl acetate	0:100	0:100	0:100	0:100	0:100	0:100	0:100	0:100	9:91
L=TBDCP									
Propene	90:10	88:12	89:11	96:4	95:5	96:4	92:8	95:5	92:8
L=DIOP									
Propene	99:1	99:1	100:0	100:0	100:0	100:0	100:0	100:0	90:10
L=ee-DIPHOS									
propene	3:97	3:97	3:97	5:95	5:95	5:95	17:83	11:89	69:31[a]
L=ea-DIPHOS									
propene	83:17	73:27	71:29	86:14	77:23	76:24	88:12	81:19	69:31[a]

[a]The data references the ea isomer of DIPHOS.

Table 3. Comparison of the approximate $\Delta\Delta E^{\ddagger}$s based on the calculated l:b ratios for ee-[Rh(H)(CO)(L)(olefin)] complexes. Experimental $\Delta\Delta E^{\ddagger}$s are an approximation of experimental l:b ratios. All $\Delta\Delta E^{\ddagger}$s are in kcal mol^{-1}.

	BLYP	BP86	PBE	B3LYP	B3P86	PBE0	B3LYP-D3	PBE0-D3	Exp[a] [63–70]
L = $(PPh_3)_2$									
Pentene	-0.96	-0.88	-0.80	-1.78	-1.74	-1.74	-3.67	-3.05	-1.74
Hexene	2.44	2.07	1.65	1.29	0.87	0.71	-3.93	-2.70	-1.44
Heptene	0.62	0.56	0.41	-0.42	-0.53	-0.66	-3.74	-2.87	-1.07
Octene	1.26	0.81	0.47	0.06	-0.42	-0.60	-4.87	-3.85	-0.85
Decene	-0.98	-1.49	-1.23	-0.08	-0.47	-0.34	3.36	2.05	-0.62
Dodecene	0.11	0.43	0.21	-0.68	-0.43	-0.54	-3.92	-2.91	-1.13
Styrene	-1.10	-1.44	-0.78	-0.94	-1.00	-1.29	5.62	2.87	1.24
Vinyl acetate	6.24	6.55	6.59	6.02	6.35	6.27	5.06	5.42	1.36
L = TBDCP									
Propene	-1.31	-1.16	-1.23	-1.86	-1.71	-1.92	-1.45	-1.70	-1.44
L = DIOP									
Propene	-2.57	-3.12	-3.22	-3.28	-3.76	-4.02	-3.59	-4.22	-1.30
L = ee-DIPHOS									
propene	2.00	2.10	2.08	1.70	1.80	1.75	0.93	1.25	-0.47[b]
L = ea-DIPHOS									
propene	-0.96	-0.58	-0.54	-1.05	-0.72	-0.69	-1.17	-0.86	-0.47[b]

[a]The $\Delta\Delta E^{\ddagger}$s shown are based on the experimental l:b ratios shown in Table 2. [b]The data references the ea isomer of DIPHOS.

For ee-[Rh(H)(CO) $(PPh_3)_2$(vinyl acetate)], the predicted $\Delta\Delta E^{\ddagger}$ was ~ 6 kcal mol^{-1} for each functional considered as shown in Table 3, indicating the branched isomer is favored. Overall, the dispersion-corrected functionals resulted in a lowering of the $\Delta\Delta E^{\ddagger}$ for ee-[Rh(H)(CO) $(PPh_3)_2$(vinyl acetate)] by approximately 1 kcal mol^{-1}, however, this did not impact the product distribution. Similarly, for ee[Rh(H)(CO)(DIOP)(propene)], the dispersion correction functionals resulted in a lowered the predicted $\Delta\Delta E^{\ddagger}$ by ~0.3 kcal mol^{-1} and did not impact the product distribution as the predicted $\Delta\Delta E^{\ddagger}$ was ~4 kcal mol^{-1}. However, for ee-[Rh(H)(CO) $(PPh_3)_2$(styrene)] and ee-[Rh(H)(CO) $(PPh_3)_2$(decene)], the dispersion-corrected functionals predicted the $\Delta\Delta E^{\ddagger}$ to be ~6 kcal/mol and ~3 kcal mol^{-1} greater than the $\Delta\Delta E^{\ddagger}$ predicted with non-dispersion-corrected functionals. While this change in $\Delta\Delta E^{\ddagger}$ predicted product ratios of 0:100 and 1:99 for B3LYP-D3 and PBE0-D3, respectively, with styrene as the olefin, with decene as the olefin, the predicted product ratios were 0:100 and 3:97 for B3LYP-D3 and PBE0-D3, respectively.

For the DIPHOS ligand, the relative orientation of the Rh-H and Rh-CO bond to the DIPHOS ligand was a major factor in predicted l:b ratios with DFT. In the ee coordination mode, all predicted l:b ratios with DFT predicted the branched product whereas the linear product is predicted for the ea coordination mode, in qualitative agreement with experiment. This is to be noted for any calculation. The small geometric changes from the ee to the ea coordination mode led to lowering of the $\Delta\Delta E^{\ddagger}$ by ~2-3 kcal mol^{-1} for all functionals, changing the product ratio to favor the linear product over the branched ratio. This exhibits the high sensitivity of $\Delta\Delta E^{\ddagger}$, which can greatly affect product formation ratios with changes as small as a few tenths of a kcal mol^{-1}, as exhibited by the $\Delta\Delta E^{\ddagger}$s of -0.54 and -1.05 kcal mol^{-1} that yielded product ratios of

71:29 and 86:14 for PBE and B3LYP, respectively. Ergo, based on the observed trends from the DFT calculations, there remains a need to investigate hydroformylation with electron correlation methods.

Table 4. Results using DLPNO methods to predict the linear-to-branched ratio for ee-[Rh(H)(CO)(DIPHOS)(propene)]

	l:b
DLPNO-MP2/aug-cc-pVDZ-PP	25:75
DLPNO-MP2/aug-cc-pVTZ-PP	29:71
DLPNO-MP2/aug-cc-pVQZ-PP	16:84
DLPNO-MP2/cc-pVTZ-PP	18:82
DLPNO-CCSD(T)/cc-pVTZ-PP	1:99
DLPNO-CCSD(T)/aug-cc-pCVDZ-PP	100:0
DLPNO-CCSD(T,FC1)/aug-cc-pCVDZ-PP	100:0
DLPNO-rp-ccCA	100:0
Experiment[a]	69:31

[a]The data references the equatorial-axial (ea) isomer of DIPHOS.

Here, the ee-[Rh(H)(CO)(DIPHOS)(propene)] catalyst-olefin complex is considered, as DFT was unable to address the regioselectivity of this reaction correctly in any case. For the DLPNO methods, the l:b ratio is predicted to favor the branched isomer except for DLPNO-CCSD(T) calculations involving the aug-cc-pCVDZ basis set. This is primarily due to the interactions between the electrons from core orbitals with electrons in valence orbitals as DLPNO-CCSD(T)/aug-cc-pCVDZ and DLPNO-CCSD(T,FC1)/aug-cc-pCVDZ, which includes sub-valence electron (FC1) excitations within the molecular orbital space, both favored the linear isomer with product ratios of 100:0. The results from implementing the DLPNO methods indicate that electronic effects from including core electrons within the valence basis set are significant in determining $\Delta\Delta E^{\ddagger}$ given the large magnitude relative to other calculated $\Delta\Delta E^{\ddagger}$s with *ab initio* methods.

Even for qualitative predictions, DLPNO-rp-ccCA is useful. By utilizing a well-described molecular orbital space – DLPNO-rp-ccCA does predict the proper regioselectivity; DFT either does not predict the correct regioselectivity, such as for ee-[Rh(H)(CO) $(PPh_3)_2$(styrene)] and ee-[Rh(H)(CO) $(PPh_3)_2$(hexene)], which predicted qualitatively inconsistent product ratios for most of the functionals examined. In addition, the regioselectivity is highly sensitive to functional choice, as the performance is not consistent as the ligand type and olefin changes. However, for the *ab initio* methods considered, simply improving the description of the molecular orbital space by including sub-valence electrons in the molecular orbital space for interactions.

3.2 Metal-ligand dissociation in organometallics. The gas phase ligand dissociation energies are shown in Table 5 with DLPNO-rp-ccCA compared to both experiment and several density functionals utilizing the resolution-of-the-identity approximation. For gas-phase ligand dissociation, DLPNO-rp-ccCA yields an error of 1.7 kcal mol^{-1} relative to experiment. When utilizing the resolution-of-the-identity approximation within DFT calculations, RI-PBE0/aug-cc-pVTZ, RI-B3LYP/aug-cc-pVTZ, and RI-TPSSh yields dissociation energies of 20.7, 20.2, and 19.6 kcal mol^{-1}, respectively. However, increasing the quality of the molecular orbital space, i.e. using aug-cc-pVQZ, increased the error by 0.4, 0.5, and 0.5 kcal mol^{-1} for RI-PBE0, RI-B3LYP, and RI-TPSSh, causing concern for utilizing DFT with higher quality basis sets. Regardless of functional and basis set choice, the predicted dissociation energy was greater than 5 kcal mol^{-1} lower than the experimental value. With the dispersion correction included for RI-PBE0/aug-cc-pVTZ, the predicted dissociation energy increased to 23.6 kcal mol^{-1}. This would suggest that accounting for dispersion is necessary for DFT predictions of gas-phase properties. DLPNO-rp-ccCA calculations yielded favorable results for ligand dissociation energy in comparison to DFT, but there are factors that can contribute to computationally predicted dissociation energies. For example, as density functionals are primarily used to generate structures for large organometallic complexes, the choice of functional for

optimization must be considered. The predicted dissociation energies can change by a few kcal mol^{-1} based on slight structural change (root mean square deviation of ~20 pm) between functionals and by 10's of kcal mol^{-1} for significant structural changes such as ligand reorientation. Also, the basis set choice can affect the quality of predictions as indicated from the lowering of predicted dissociation energy by increasing basis set quality.

Table 5. A comparison of the gas-phase ligand dissociation energy of H_2O from the Pt complex calculated with DLPNO-rp-ccCA and RI-DFT/aug-cc-pVnZ. All energies are in kcal mol^{-1} and are BSSE-corrected.

RI-PBE0/aug-cc-pVTZ	20.7
RI-B3LYP/aug-cc-pVTZ	20.2
RI-TPSSh/aug-cc-pVTZ	19.6
RI-PBE0/aug-cc-pVQZ	20.3
RI-B3LYP/aug-cc-pVQZ	19.7
RI-TPSSh/aug-cc-pVQZ	19.1
RI-PBE0-D3/aug-cc-pVTZ	23.6
DLPNO-rp-ccCA	24.2
Experiment	25.9 ± 0.7

4. Conclusion

There are numerous challenges in the prediction of thermochemistry properties for transition metal species as illustrated in this examination of regioselectivity and ligand dissociation energy. And, thus, gauging the utility of computational method, considering metal, ligand, and property, is essential. A typical method choice for the study of transition metal species is DFT. Unfortunately, there is no "magic" computational approach to use for all problems. While *ab initio* methods like CCSD(T) or composite methods that try to replicate it like ccCA can be quite useful and are more dependable from system to system and, generally, across a reaction pathway, they are more costly, and may require additional measures to ensure quality results are obtained sometimes reaching near saturation of the orbital space (even more costly!). DFT can be very useful, but properly gauging it is important, as illustrated by this study.

Acknowledgements
This material is based upon work supported by the National Science Foundation under Grant No. CHE-1362479/DMR-1636557. Computational resources were provided via the NSF Major Research Instrumentation program supported by the National Science Foundation under Grant No. CHE-1531468. A very special thanks to Peter Margl and his colleagues at Dow Chemical who first motivated some of our work in this area.

REFERENCES

[1] A. Karton, S. Daon, J.M.L. Martin, W4-11: A high-confidence benchmark dataset for computational thermochemistry derived from first-principles W4 data, Chem. Phys. Lett. 510 (2011) 165–178. doi:10.1016/j.cplett.2011.05.007.

[2] T.R. Cundari, H. Arturo Ruiz Leza, T. Grimes, G. Steyl, A. Waters, A.K. Wilson, Calculation of the enthalpies of formation for transition metal complexes, Chem. Phys. Lett. 401 (2005) 58–61. doi:10.1016/j.cplett.2004.11.021.

[3] S.M. Tekarli, M.L. Drummond, T.G. Williams, T.R. Cundari, A.K. Wilson, Performance of Density Functional Theory for 3d Transition Metal-Containing Complexes: Utilization of the Correlation Consistent Basis Sets, J. Phys. Chem. A. 113 (2009) 8607–8614. doi:10.1021/jp811503v.

[4] W. Jiang, M.L. Laury, M. Powell, A.K. Wilson, Comparative Study of Single and Double Hybrid Density Functionals for the Prediction of 3d Transition Metal Thermochemistry, J. Chem. Theory Comput. 8 (2012) 4102–4111. doi:10.1021/ct300455e.

[5] M.L. Laury, A.K. Wilson, Performance of Density Functional Theory for Second Row (4 d) Transition Metal Thermochemistry, J. Chem. Theory Comput. 9 (2013) 3939–3946. doi:10.1021/ct400379z.

[6] J.J. Determan, K. Poole, G. Scalmani, M.J. Frisch, B.G. Janesko, A.K. Wilson, Comparative Study of Nonhybrid Density Functional Approximations for the Prediction of 3d Transition Metal Thermochemistry, J. Chem. Theory Comput. 13 (2017) 4907–4913. doi:10.1021/acs.jctc.7b00809.

[7] Y. Zhao, D.G. Truhlar, Comparative assessment of density functional methods for 3d transition-metal chemistry, J. Chem. Phys. 124 (2006) 1–7. doi:10.1063/1.2202732.

[8] S. Dohm, A. Hansen, M. Steinmetz, S. Grimme, M.P. Checinski, Comprehensive Thermochemical Benchmark Set of Realistic Closed-Shell Metal Organic Reactions, J. Chem. Theory Comput. 14 (2018) 2596–2608. doi:10.1021/acs.jctc.7b01183.

[9] N.J. DeYonker, T.R. Cundari, A.K. Wilson, The correlation consistent composite approach (ccCA): An alternative to the Gaussian-n methods, J. Chem. Phys. 124 (2006) 114104. doi:10.1063/1.2173988.

[10] M.L. Laury, N.J. DeYonker, W. Jiang, A.K. Wilson, A pseudopotential-based composite method: The relativistic pseudopotential correlation consistent composite approach for molecules containing 4d transition metals (Y-Cd), J. Chem. Phys. 135 (2011) 214103. doi:10.1063/1.3662415.

[11] S.A. Nedd, N.J. DeYonker, A.K. Wilson, P. Piecuch, M.S. Gordon, Incorporating a completely renormalized coupled cluster approach into a composite method for thermodynamic properties and reaction paths, J. Chem. Phys. 136 (2012) 144109. doi:10.1063/1.3700801.

[12] W. Jiang, N.J. DeYonker, J.J. Determan, A.K. Wilson, Toward accurate theoretical thermochemistry of first row transition metal complexes, J. Phys. Chem. A. 116 (2012) 870–885. doi:10.1021/jp205710e.

[13] S. Manivasagam, M.L. Laury, A.K. Wilson, Pseudopotential-Based Correlation Consistent Composite Approach (rp-ccCA) for First- and Second-Row Transition Metal Thermochemistry, J. Phys. Chem. A. 119 (2015) 6867–6874. doi:10.1021/acs.jpca.5b02433.

[14] D. Evans, J.A. Osborn, G. Wilkinson, Hydroformylation of alkenes by use of rhodium complex catalysts, J. Chem. Soc. A Inorganic, Phys. Theor. (1968) 3133. doi:10.1039/j19680003133.

[15] J. Klosin, C.R. Landis, Ligands for practical rhodium-catalyzed asymmetric hydroformylation, Acc. Chem. Res. 40 (2007) 1251–1259. doi:10.1021/ar7001039.

[16] I.A. Tonks, R.D.J. Froese, C.R. Landis, Very low pressure Rh-catalyzed hydroformylation of styrene with (S,S,S-bisdiazaphos): Regioselectivity inversion and mechanistic insights, ACS Catal. 3 (2013) 2905–2909. doi:10.1021/cs400943s.

[17] M. Kranenburg, Y.E.M. van der Burgt, P.C.J. Kamer, P.W.N.M. van Leeuwen, K. Goubitz, J. Fraanje, New Diphosphine Ligands Based on Heterocyclic Aromatics Inducing Very High

Regioselectivity in Rhodium-Catalyzed Hydroformylation: Effect of the Bite Angle, Organometallics. 14 (1995) 3081–3089. doi:10.1021/om00006a057.
[18] S.A. Decker, T.R. Cundari, Hybrid QM/MM study of propene insertion into the Rh-H bond of HRh(PPh3)2(CO)(η2-CH2=CHCH3): The role of the olefin adduct in determining product selectivity, J. Organomet. Chem. 635 (2001) 132–141. doi:10.1016/S0022-328X(01)01065-8.
[19] S.A. Decker, T.R. Cundari, DFT Study of the Ethylene Hydroformylation Catalytic Cycle Employing a HRh(PH $_3$) $_2$ (CO) Model Catalyst, Organometallics. 20 (2001) 2827–2841. doi:10.1021/om010019q.
[20] J.J. Carbó, F. Maseras, C. Bo, P.W.N.M. van Leeuwen, Unraveling the Origin of Regioselectivity in Rhodium Diphosphine Catalyzed Hydroformylation. A DFT QM/MM Study, J. Am. Chem. Soc. 123 (2001) 7630–7637. doi:10.1021/ja0101678.
[21] C.R. Landis, J. Uddin, Quantum mechanical modelling of alkene hydroformylation as catalyzed by xantphos-Rh complexesBased on the presentation given at Dalton Discussion No. 4, 10–13th January 2002, Kloster Banz, Germany., J. Chem. Soc. Dalt. Trans. (2002) 729–742. doi:10.1039/b108649a.
[22] M.A. Carvajal, S. Kozuch, S. Shaik, Factors Controlling the Selective Hydroformylation of Internal Alkenes to Linear Aldehydes. 1. The Isomerization Step, Organometallics. 28 (2009) 3656–3665. doi:10.1021/om801166x.
[23] U. Gellrich, D. Himmel, M. Meuwly, B. Breit, Realistic energy surfaces for real-world systems: An IMOMO CCSD(T):DFT scheme for rhodium-catalyzed hydroformylation with the 6-dppon ligand, Chem. - A Eur. J. 19 (2013) 16272–16281. doi:10.1002/chem.201302132.
[24] M. Kumar, R. V. Chaudhari, B. Subramaniam, T.A. Jackson, Ligand effects on the regioselectivity of rhodium-catalyzed hydroformylation: Density functional calculations illuminate the role of long-range noncovalent interactions, Organometallics. 33 (2014) 4183–4191. doi:10.1021/om500196g.
[25] I. Jacobs, B. De Bruin, J.N.H. Reek, Comparison of the full catalytic cycle of hydroformylation mediated by mono- and bis-ligated triphenylphosphine-rhodium complexes by using DFT calculations, ChemCatChem. 7 (2015) 1708–1718. doi:10.1002/cctc.201500087.
[26] M.D. Wodrich, M. Busch, C. Corminboeuf, Expedited Screening of Active and Regioselective Catalysts for the Hydroformylation Reaction, Helv. Chim. Acta. 101 (2018). doi:10.1002/hlca.201800107.
[27] M. Svensson, S. Humbel, R.D.J. Froese, T. Matsubara, S. Sieber, K. Morokuma, ONIOM: A Multilayered Integrated MO + MM Method for Geometry Optimizations and Single Point Energy Predictions. A Test for Diels−Alder Reactions and Pt(P(*t* -Bu) $_3$) $_2$ + H $_2$ Oxidative Addition, J. Phys. Chem. 100 (1996) 19357–19363. doi:10.1021/jp962071j.
[28] S. Dapprich, I. Komáromi, K.S. Byun, K. Morokuma, M.J. Frisch, A new ONIOM implementation in Gaussian98. Part I. The calculation of energies, gradients, vibrational frequencies and electric field derivatives, J. Mol. Struct. THEOCHEM. 461–462 (1999) 1–21. doi:10.1016/S0166-1280(98)00475-8.
[29] L.E. Rush, P.G. Pringle, J.N. Harvey, Computational Kinetics of Cobalt-Catalyzed Alkene Hydroformylation, Angew. Chemie Int. Ed. 53 (2014) 8672–8676. doi:10.1002/anie.201402115.
[30] M. Kumar, R. V. Chaudhari, B. Subramaniam, T.A. Jackson, Importance of Long-Range Noncovalent Interactions in the Regioselectivity of Rhodium-Xantphos-Catalyzed Hydroformylation, Organometallics. 34 (2015) 1062–1073. doi:10.1021/om5012775.
[31] J.R. Kitchin, Machine learning in catalysis, Nat. Catal. 1 (2018) 230–232. doi:10.1038/s41929-018-0056-y.
[32] J.A. Labinger, J.E. Bercaw, Understanding and exploiting C–H bond activation, Nature. 417 (2002) 507–514. doi:10.1038/417507a.
[33] S.S. Stahl, J.A. Labinger, J.E. Bercaw, Homogeneous Oxidation of Alkanes by Electrophilic Late Transition Metals, Angew. Chemie Int. Ed. 37 (1998) 2180–2192. doi:10.1002/(SICI)1521-3773(19980904)37:16<2180::AID-ANIE2180>3.0.CO;2-A.

[34] L.A. Hammad, G. Gerdes, P. Chen, Determination of Ligand Binding Energies in Platinum (II) Complexes, (2005) 1907–1913.
[35] J. Hartwig, Organotransition Metal Chemistry: From Bonding to Catalysis, University Science Books, Sausalito, California, 2010.
[36] A.D. Becke, Density-functional thermochemistry. III. The role of exact exchange, J. Chem. Phys. 98 (1993) 5648–5652. doi:10.1063/1.464913.
[37] C. Lee, W. Yang, R.G. Parr, Development of the Colle-Salvetti correlation-energy formula into a functional of the electron density, Phys. Rev. B. 37 (1988) 785–789. doi:10.1103/PhysRevB.37.785.
[38] J.P. Perdew, Density-functional approximation for the correlation energy of the inhomogeneous electron gas, Phys. Rev. B. 33 (1986) 8822–8824. doi:10.1103/PhysRevB.33.8822.
[39] A.D. Becke, Density-functional exchange-energy approximation with correct asymptotic behavior, Phys. Rev. A. 38 (1988) 3098–3100. doi:10.1103/PhysRevA.38.3098.
[40] J.P. Perdew, K. Burke, M. Ernzerhof, Generalized gradient approximation made simple, Phys. Rev. Lett. 77 (1996) 3865–3868. doi:10.1103/PhysRevLett.77.3865.
[41] M. Ernzerhof, G.E. Scuseria, Assessment of the Perdew-Burke-Ernzerhof exchange-correlation functional, J. Chem. Phys. 110 (1999) 5029–5036. doi:10.1063/1.478401.
[42] C. Adamo, V. Barone, Toward reliable density functional methods without adjustable parameters: The PBE0 model, J. Chem. Phys. 110 (1999) 6158–6170. doi:10.1063/1.478522.
[43] S. Grimme, J. Antony, S. Ehrlich, H. Krieg, A consistent and accurate ab initio parametrization of density functional dispersion correction (DFT-D) for the 94 elements H-Pu, J. Chem. Phys. 132 (2010) 154104. doi:10.1063/1.3382344.
[44] G. Igel-Mann, H. Stoll, H. Preuß, Pseudopotential study of monohydrides and monoxides of main group elements K through Br, Mol. Phys. 65 (1988) 1329–1336. doi:10.1080/00268978800101821.
[45] D. Andrae, U. Häußermann, M. Dolg, H. Stoll, H. Preuß, Energy-adjusted ab initio pseudopotentials for the second and third row transition elements, Theor. Chem. Acc. 77 (1990) 123–141. doi:10.1007/BF01114537.
[46] M.J. Frisch, G.W. Trucks, H.B. Schlegel, G.E. Scuseria, M.A. Robb, J.R. Cheeseman, G. Scalmani, V. Barone, G.A. Petersson, H. Nakatsuji, X. Li, M. Caricato, A. V. Marenich, J. Bloino, B.G. Janesko, R. Gomperts, B. Mennucci, H.P. Hratchian, J. V. Ortiz, A.F. Izmaylov, J.L. Sonnenberg, D. Williams-Young, F. Ding, F. Lipparini, F. Egidi, J. Goings, B. Peng, A. Petrone, T. Henderson, D. Ranasinghe, V.G. Zakrzewski, J. Gao, N. Rega, G. Zheng, W. Liang, M. Hada, M. Ehara, K. Toyota, R. Fukuda, J. Hasegawa, M. Ishida, T. Nakajima, Y. Honda, O. Kitao, H. Nakai, T. Vreven, K. Throssell, J.A. Montgomery Jr., J.E. Peralta, F. Ogliaro, M.J. Bearpark, J.J. Heyd, E.N. Brothers, K.N. Kudin, V.N. Staroverov, T.A. Keith, R. Kobayashi, J. Normand, K. Raghavachari, A.P. Rendell, J.C. Burant, S.S. Iyengar, J. Tomasi, M. Cossi, J.M. Millam, M. Klene, C. Adamo, R. Cammi, J.W. Ochterski, R.L. Martin, K. Morokuma, O. Farkas, J.B. Foresman, D.J. Fox, Gaussian 16, Revision A.03, (2016) 2016. doi:.
[47] C. Riplinger, F. Neese, An efficient and near linear scaling pair natural orbital based local coupled cluster method, J. Chem. Phys. 138 (2013) 034106. doi:10.1063/1.4773581.
[48] C. Riplinger, B. Sandhoefer, A. Hansen, F. Neese, Natural triple excitations in local coupled cluster calculations with pair natural orbitals, J. Chem. Phys. 139 (2013) 134101. doi:10.1063/1.4821834.
[49] P. Pinski, C. Riplinger, E.F. Valeev, F. Neese, Sparse maps - A systematic infrastructure for reduced-scaling electronic structure methods. I. An efficient and simple linear scaling local MP2 method that uses an intermediate basis of pair natural orbitals, J. Chem. Phys. 143 (2015) 034108. doi:10.1063/1.4926879.
[50] C. Riplinger, P. Pinski, U. Becker, E.F. Valeev, F. Neese, Sparse maps - A systematic infrastructure for reduced-scaling electronic structure methods. II. Linear scaling domain based pair natural orbital coupled cluster theory, J. Chem. Phys. 144 (2016). doi:10.1063/1.4939030.

[51] F. Pavošević, C. Peng, P. Pinski, C. Riplinger, F. Neese, E.F. Valeev, SparseMaps - A systematic infrastructure for reduced scaling electronic structure methods. V. Linear scaling explicitly correlated coupled-cluster method with pair natural orbitals, J. Chem. Phys. 146 (2017). doi:10.1063/1.4979993.
[52] M. Saitow, U. Becker, C. Riplinger, E.F. Valeev, F. Neese, A new near-linear scaling, efficient and accurate, open-shell domain-based local pair natural orbital coupled cluster singles and doubles theory, J. Chem. Phys. 146 (2017) 164105. doi:10.1063/1.4981521.
[53] F. Neese, Software update: the ORCA program system, version 4.0, Wiley Interdiscip. Rev. Comput. Mol. Sci. 8 (2018) e1327. doi:10.1002/wcms.1327.
[54] T.H. Dunning Jr., Gaussian basis sets for use in correlated molecular calculations. I. The atoms boron through neon and hydrogen, J. Chem. Phys. 90 (1989) 1007–1023. doi:10.1063/1.456153.
[55] T.H. Dunning Jr., K.A. Peterson, A.K. Wilson, Gaussian basis sets for use in correlated molecular calculations. X. The atoms aluminum through argon revisited, J. Chem. Phys. 114 (2001) 9244–9253. doi:10.1063/1.1367373.
[56] K.A. Peterson, D. Figgen, M. Dolg, H. Stoll, Energy-consistent relativistic pseudopotentials and correlation consistent basis sets for the 4d elements Y-Pd, J. Chem. Phys. 126 (2007) 124101. doi:10.1063/1.2647019.
[57] D. Figgen, K.A. Peterson, M. Dolg, H. Stoll, Energy-consistent pseudopotentials and correlation consistent basis sets for the 5d elements Hf-Pt, J. Chem. Phys. 130 (2009) 164108. doi:10.1063/1.3119665.
[58] P. Patel, A.K. Wilson, Utilization of the Domain-Based Local Pair Natural Orbital Methods within the correlation consistent Composite Approach, (Submitted). (2019).
[59] A. V. Marenich, C.J. Cramer, D.G. Truhlar, Universal Solvation Model Based on Solute Electron Density and on a Continuum Model of the Solvent Defined by the Bulk Dielectric Constant and Atomic Surface Tensions, J. Phys. Chem. B. 113 (2009) 6378–6396. doi:10.1021/jp810292n.
[60] S.F. Boys, F. Bernardi, The calculation of small molecular interactions by the differences of separate total energies. Some procedures with reduced errors, Mol. Phys. 19 (1970) 553–566. doi:10.1080/00268977000101561.
[61] T. Weymuth, E.P.A. Couzijn, P. Chen, M. Reiher, New benchmark set of transition-metal coordination reactions for the assessment of density functionals, J. Chem. Theory Comput. 10 (2014) 3092–3103. doi:10.1021/ct500248h.
[62] V.N. Staroverov, G.E. Scuseria, J. Tao, J.P. Perdew, Comparative assessment of a new nonempirical density functional: Molecules and hydrogen-bonded complexes, J. Chem. Phys. 119 (2003) 12129–12137. doi:10.1063/1.1626543.
[63] D. Evans, J.A. Osborn, G. Wilkinson, Hydroformylation of alkenes by use of rhodium complex catalysts, J. Chem. Soc. A Inorganic, Phys. Theor. 566 (1968) 3133. doi:10.1039/j19680003133.
[64] C.K. Brown, G. Wilkinson, Homogeneous hydroformylation of alkenes with hydridocarbonyltris-(triphenylphosphine)rhodium(I) as catalyst., J. Chem. Soc. A Inorganic, Phys. Theor. (1970) 2753. doi:10.1039/j19700002753.
[65] P.W.N.M. van Leeuwen, N.D. Clément, M.J.-L. Tschan, New processes for the selective production of 1-octene, Coord. Chem. Rev. 255 (2011) 1499–1517. doi:10.1016/j.ccr.2010.10.009.
[66] R.M. Deshpande, S.S. Divekar, R. V. Gholap, R. V. Chaudhari, Enhancement of rate and selectivity in hydroformylation of allyl alcohol through solvent effect, Ind. Eng. Chem. Res. 30 (1991) 1389–1390. doi:10.1021/ie00054a047.
[67] J.T. Carlock, A comparative study of triphenylamine, triphenylphosphine, triphenylarsine, triphenylantimony and triphenylbismuth as ligands in the rhodium-catal yzed hydroformylation of 1-dodecene, Tetrahedron. 40 (1984) 185–187. doi:10.1016/0040-4020(84)85118-2.
[68] Y.L. Borole, R. V. Chaudhari, New Route for the Synthesis of Propylene Glycols via Hydroformylation of Vinyl Acetate, Ind. Eng. Chem. Res. 44 (2005) 9601–9608. doi:10.1021/ie050272g.
[69] C.P. Casey, G.T. Whiteker, M.G. Melville, L.M. Petrovich, J.A. Gavney, D.R. Powell,

Diphosphines with natural bite angles near 120.degree. increase selectivity for n-aldehyde formation in rhodium-catalyzed hydroformylation, J. Am. Chem. Soc. 114 (1992) 5535–5543. doi:10.1021/ja00040a008.

[70] C.P. Casey, L.M. Petrovich, (Chelating diphosphine)rhodium-Catalyzed Deuterioformylation of 1-Hexene: Control of Regiochemistry by the Kinetic Ratio of Alkylrhodium Species Formed by Hydride Addition to Complexed Alkene, J. Am. Chem. Soc. 117 (1995) 6007–6014. doi:10.1021/ja00127a014.

Table

Table 1. A summary of the effect of $\Delta\Delta E^{\ddagger}$ in kcal mol^{-1} on the linear-to-branched ratio (l:b) ratio for hydroformylation.

$\Delta\Delta E^{\ddagger}$ (kcal mol^{-1})	Linear-to-branched ratio (l:b)
0 to -1	50:50 to 84:16
1 to -2	84:16 to 97:3
-2 to -3	97:3 to 100:0

Table

Table 2. A comparison of several density functionals to linear-to-branched ratios from experiment for ee-[Rh(H)(CO)(L)(olefin)] complexes

	BLYP	BP86	PBE	B3LYP	B3P86	PBE0	B3LYP-D3	PBE0-D3	Exp [63–70]
L=$(PPh_3)_2$									
Pentene	83:17	81:19	79:21	95:5	95:5	95:5	100:0	99:1	95:5
Hexene	2:98	3:97	6:94	10:90	19:81	23:77	100:0	99:1	92:8
Heptene	26:74	28:72	33:67	67:33	71:29	75:25	100:0	99:1	86:14
Octene	11:89	20:80	31:69	47:53	67:33	73:27	100:0	100:0	81:19
Decene	84:16	93:7	89:11	53:47	69:31	64:36	0:100	3:97	74:26
Dodecene	45:55	33:67	41:59	76:24	68:32	71:29	100:0	99:1	87:12
Styrene	87:13	92:8	79:21	83:17	84:16	90:10	0:100	1:99	11:89
Vinyl acetate	0:100	0:100	0:100	0:100	0:100	0:100	0:100	0:100	9:91
L=TBDCP									
Propene	90:10	88:12	89:11	96:4	95:5	96:4	92:8	95:5	92:8
L=DIOP									
Propene	99:1	99:1	100:0	100:0	100:0	100:0	100:0	100:0	90:10
L=ee-DIPHOS									
propene	3:97	3:97	3:97	5:95	5:95	5:95	17:83	11:89	69:31[a]
L=ea-DIPHOS									
propene	83:17	73:27	71:29	86:14	77:23	76:24	88:12	81:19	69:31[a]

[a]The data references the ea conformer of DIPHOS.

Table

Table 3. A comparison of the approximate $\Delta\Delta E^{\ddagger}$s based on the calculated l:b ratios for ee-[Rh(H)(CO)(L)(olefin)] complexes. Experimental $\Delta\Delta E^{\ddagger}$s are an approximation of experimental l:b ratios. All $\Delta\Delta E^{\ddagger}$s are in kcal mol^{-1}.

	BLYP	BP86	PBE	B3LYP	B3P86	PBE0	B3LYP-D3	PBE0-D3	Exp[a] [63–70]
L = $(PPh_3)_2$									
Pentene	-0.96	-0.88	-0.80	-1.78	-1.74	-1.74	-3.67	-3.05	-1.74
Hexene	2.44	2.07	1.65	1.29	0.87	0.71	-3.93	-2.70	-1.44
Heptene	0.62	0.56	0.41	-0.42	-0.53	-0.66	-3.74	-2.87	-1.07
Octene	1.26	0.81	0.47	0.06	-0.42	-0.60	-4.87	-3.85	-0.85
Decene	-0.98	-1.49	-1.23	-0.08	-0.47	-0.34	3.36	2.05	-0.62
Dodecene	0.11	0.43	0.21	-0.68	-0.43	-0.54	-3.92	-2.91	-1.13
Styrene	-1.10	-1.44	-0.78	-0.94	-1.00	-1.29	5.62	2.87	1.24
Vinyl acetate	6.24	6.55	6.59	6.02	6.35	6.27	5.06	5.42	1.36
L = TBDCP									
Propene	-1.31	-1.16	-1.23	-1.86	-1.71	-1.92	-1.45	-1.70	-1.44
L = DIOP									
Propene	-2.57	-3.12	-3.22	-3.28	-3.76	-4.02	-3.59	-4.22	-1.30
L = ee-DIPHOS									
propene	2.00	2.10	2.08	1.70	1.80	1.75	0.93	1.25	-0.47[b]
L = ea-DIPHOS									
propene	-0.96	-0.58	-0.54	-1.05	-0.72	-0.69	-1.17	-0.86	-0.47[b]

[a]The $\Delta\Delta E^{\ddagger}$s shown are based on the experimental l:b ratios shown in Table 2. [b]The data references the ea conformer of DIPHOS.

Table

Table 4. Results using DLPNO methods to predict the linear-to-branched ratio for ee-[Rh(H)(CO)(DIPHOS)(propene)]

	l:b
DLPNO-MP2/aug-cc-pVDZ-PP	25:75
DLPNO-MP2/aug-cc-pVTZ-PP	29:71
DLPNO-MP2/aug-cc-pVQZ-PP	16:84
DLPNO-MP2/cc-pVTZ-PP	18:82
DLPNO-CCSD(T)/cc-pVTZ-PP	1:99
DLPNO-CCSD(T)/aug-cc-pCVDZ-PP	100:0
DLPNO-CCSD(T,FC1)/aug-cc-pCVDZ-PP	100:0
DLPNO-rp-ccCA	100:0
Experiment[a]	69:31

[a]The data references the equatorial-axial (ea) isomer of DIPHOS.

Table

Table 5. A comparison of the gas-phase ligand dissociation energy of H_2O from the Pt complex calculated with DLPNO-rp-ccCA and RI-DFT/aug-cc-pVnZ. All energies are in kcal mol^{-1} and are BSSE-corrected.

RI-PBE0/aug-cc-pVTZ	20.7
RI-B3LYP/aug-cc-pVTZ	20.2
RI-TPSSh/aug-cc-pVTZ	19.6
RI-PBE0/aug-cc-pVQZ	20.3
RI-B3LYP/aug-cc-pVQZ	19.7
RI-TPSSh/aug-cc-pVQZ	19.1
RI-PBE0-D3/aug-cc-pVTZ	23.6
DLPNO-rp-ccCA	24.2
Experiment	25.9 ± 0.7

Figure

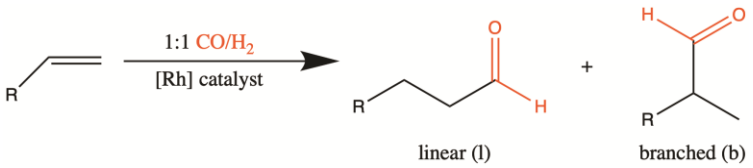

Figure 1. The hydroformylation reaction converting olefins to linear and branched aldehydes via a Rh catalyst.

Figure

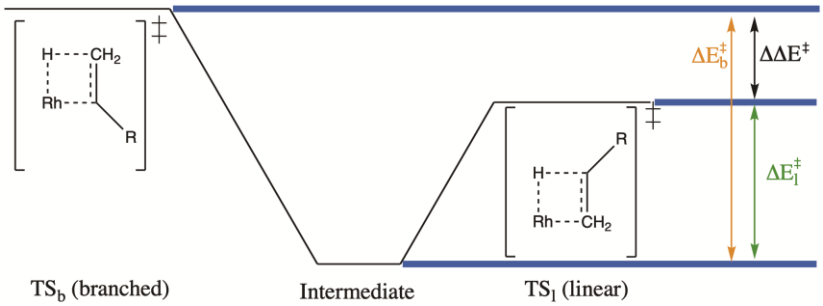

Figure 2. A model of the two reaction pathways for hydroformylation where $\Delta E_l^{\ddagger}$ and $\Delta E_b^{\ddagger}$ are the reaction barrier for forming the linear and branched product, respectively. $\Delta\Delta E^{\ddagger}$ is the difference in energy between the two reaction barriers.

Figure

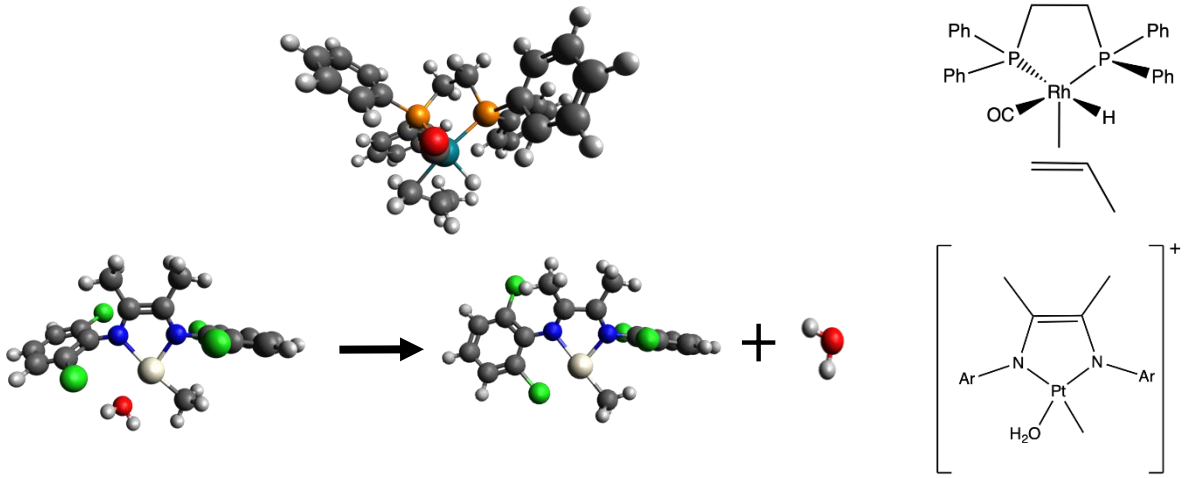

Figure 3. Computationally determined 3D structures (left) and 2D structures (right) of ee-[Rh(H)(CO)(DIPHOS)(propene)] catalyst complex (top) and dissociation reaction of H_2O from the cationic (diimine)(aquo)Pt^{II} complex (bottom). Ph=Phenyl and Ar=2,6-dichlorobenzene. Pt=Silver, N=Blue, O=Red, C=Dark Gray, H=Light Gray, Cl=Green, P=Orange, Rh=Teal.

Figure

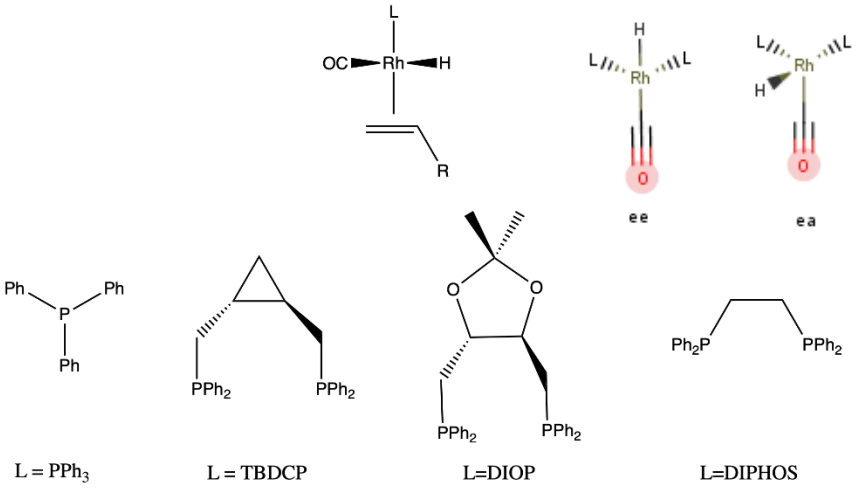

Figure 4. 2D structures of the monodentate and bidentate ligands for hydroformylation as well as the equatorial-equatorial (ee) and equatorial-axial (ea) conformations of the [Rh(H)(CO)] backbone. All ligands are bound to a [Rh(H)(CO)] backbone.

3D Models (.zip)

Click here to access/download
3D Models (.zip)
3Dcoord_XYZ.zip